JCI insight

RESEARCH ARTICLE

Enapotamab vedotin, an AXL-specific antibody-drug conjugate, shows preclinical antitumor activity in non-small cell lung cancer

Louise A. Koopman,[1] Mikkel G. Terp,[2] Gijs G. Zom,[1] Maarten L. Janmaat,[1] Kirstine Jacobsen,[2] Elke Gresnigt-van den Heuvel,[1] Marcel Brandhorst,[1] Ulf Forssmann,[1] Freddy de Bree,[1] Nora Pencheva,[1] Andreas Lingnau,[1] Maria A. Zipeto,[3] Paul W.H.I Parren,[1,2,4] Esther C.W. Breij,[1] and Henrik J. Ditzel[2,5]

[1]Genmab, Utrecht, Netherlands. [2]Department of Cancer and Inflammation Research, Institute of Molecular Medicine, University of Southern Denmark, Odense, Denmark. [3]Crown Bioscience San Diego, San Diego, California, USA. [4]Department of Immunohematology and Blood Transfusion, Leiden University Medical Center, Leiden, Netherlands. [5]Department of Oncology, Odense University Hospital, Odense, Denmark.

Targeted therapies and immunotherapy have shown promise in patients with non-small cell lung cancer (NSCLC). However, the majority of patients fail or become resistant to treatment, emphasizing the need for novel treatments. In this study, we confirm the prognostic value of levels of AXL, a member of the TAM receptor tyrosine kinase family, in NSCLC and demonstrate potent antitumor activity of the AXL-targeting antibody-drug conjugate enapotamab vedotin across different NSCLC subtypes in a mouse clinical trial of human NSCLC. Tumor regression or stasis was observed in 17/61 (28%) of the patient-derived xenograft (PDX) models and was associated with AXL mRNA expression levels. Significant single-agent activity of enapotamab vedotin was validated in vivo in 9 of 10 AXL-expressing NSCLC xenograft models. In a panel of *EGFR*-mutant NSCLC cell lines rendered resistant to *EGFR* inhibitors in vitro, we observed de novo or increased AXL protein expression concomitant with enapotamab vedotin–mediated cytotoxicity. Enapotamab vedotin also showed antitumor activity in vivo in 3 *EGFR*-mutant, EGFR inhibitor–resistant PDX models, including an osimertinib-resistant NSCLC PDX model. In summary, enapotamab vedotin has promising therapeutic potential in NSCLC. The safety and preliminary efficacy of enapotamab vedotin are currently being evaluated in the clinic across multiple solid tumor types, including NSCLC.

Authorship note: LAK and MGT contributed equally to this work. ECWB and HJD contributed equally to this work.

Conflict of interest: LAK, GGZ, MLJ, EGVDH, MB, UF, FDB, NP, AL, and ECWB are employees of Genmab, receive a salary from Genmab, and declare ownership of restricted stock units and/or warrants from Genmab, and PWHIP is a Genmab shareholder.

Submitted: February 25, 2019
Accepted: September 25, 2019
Published: November 1, 2019.

Reference information: *JCI Insight*. 2019;4(21):e128199. https://doi.org/10.1172/jci.insight.128199.

Introduction

Lung cancer is the most commonly diagnosed cancer and the leading cause of cancer mortality worldwide (1). Less than 20% of patients with advanced non-small cell lung cancer (NSCLC) live longer than 5 years after diagnosis (2). For decades, standard treatment consisted of platinum-based combination chemotherapy and radiotherapy. Recent advances in immunotherapy have broadened the treatment options, as evident in the approval of pembrolizumab as first-line therapy in *EGFR*–wild-type NSCLC patients (3). In addition, the development of tyrosine kinase inhibitors targeting EGFR has significantly increased the survival of a subset of NSCLC patients who harbor tumors with activating *EGFR* mutations, which account for 10%–20% of NSCLC patients in Europe and North America and 50%–60% of East Asian patients (4–7).

AXL, a member of the TYRO3, AXL, and MERTK (TAM) family of receptor tyrosine kinases (RTKs), has been associated with phenotype switching from a proliferative to a more invasive phenotype and epithelial-mesenchymal transition (EMT) in cancer. Aberrant expression of AXL has been described in a multitude of malignancies, including NSCLC (8, 9). In transcriptomic analyses of a large NSCLC cell line panel, AXL overexpression was particularly noted in the subset with an EMT-like gene signature, which frequently harbors *KRAS* mutations, whereas *EGFR* mutations are restricted to the epithelial subset (8). On the other hand, enhanced expression of AXL was observed in 20% of NSCLC patients

with EGFR inhibitor (EGFRi) drug resistance, both of which are typically associated with the mesenchymal phenotype (9). In other cancer types, overexpression of AXL has been associated with intrinsic or acquired resistance to PI3K inhibitors, anti-HER2 treatment, and immune checkpoint inhibitors, as well as resistance to chemotherapy and radiotherapy (10–12). Because of its key role in tumorigenesis and drug resistance, AXL has emerged as an attractive target for cancer therapy. Several AXL-targeting small molecules and antibody-based therapies, either alone or in combination with other drugs, are in preclinical and clinical development (13).

AXL-targeting therapies may be of clinical benefit in all patients with NSCLC, both those bearing tumors that are *EGFR* wild-type with mesenchymal features and frequent *KRAS* mutations and those whose tumors contain *EGFR*-activating mutations and become resistant to targeted EGFRi. Although almost 70% of patients with *EGFR*-mutant NSCLC respond to first-line treatment, complete responses are rare and nearly all develop resistance and ultimately succumb to the disease (14). An array of resistance mechanisms against *EGFR*-targeted therapy have been identified and include secondary mutations in *EGFR* as well as amplification, overexpression, and autocrine loops of alternative parallel tumor-promoting pathways involving, e.g., MET protooncogene (MET), the AKT pathway, and RTKs MERTK and AXL (9, 15–19).

Enapotamab vedotin (previously referred to as HuMax-AXL-ADC or AXL-107-MMAE) is a clinical-stage AXL-specific antibody-drug conjugate that was generated by conjugating a human AXL-specific IgG1 with the microtubule-disrupting agent monomethyl auristatin E (MMAE) via a protease-cleavable valine-citrulline linker. For optimal potency, enapotamab vedotin depends on AXL expression but does not compete with, and is as such independent of, activation of AXL signaling by its ligand, Gas6 (20). We recently demonstrated promising antitumor effects of enapotamab vedotin in patient-derived xenograft (PDX) models representing a variety of solid cancers, including lung, pancreas, thyroid, esophageal, and cervical cancer and malignant melanoma (20). Furthermore, we showed that subpopulations of AXL^+, MAPK pathway inhibitor–resistant melanoma cells, enriched under the selective pressure of MAPK inhibitor treatment, were effectively eliminated by enapotamab vedotin in preclinical experiments (20). The clinical safety and preliminary efficacy of enapotamab vedotin are currently being evaluated in a phase I/II study (ClinicalTrials.org identifier: NCT02988817) in solid cancers, including NSCLC with and without *EGFR* mutations.

In the present study, we investigated the prognostic value of AXL expression in primary tumor tissues of patients with NSCLC and assessed the antitumor activity of enapotamab vedotin across the NSCLC population by performing a mouse clinical trial comprising NSCLC PDX models, representing different histological and mutational subtypes. Moreover, in view of existing evidence of increased AXL expression in *EGFR*-mutant, treatment-resistant NSCLC, we hypothesized that increased AXL expression in NSCLC models with acquired resistance to EGFRi, including the third-generation EGFRi osimertinib, would be associated with sensitivity to enapotamab vedotin treatment. We tested this, both in vitro using a cell line panel with in vitro–acquired EGFRi resistance and in vivo in PDX models. These PDX models were derived either from clinically EGFRi-resistant *EGFR*-mutant NSCLC patients or from xenograft-bearing mice rendered resistant to EGFRi preclinically through continuous exposure to EGFRi.

Results

AXL expression levels in NSCLC patient tumors correlate with clinical outcome. To establish the clinical relevance of AXL expression in NSCLC tumors, we assessed AXL expression in comprehensive cohorts of NSCLC tumors through IHC-based and transcriptomic approaches. Initially, we evaluated AXL protein expression in a testing cohort of primary NSCLC tissues (n = 117, Supplemental Table 1; supplemental material available online with this article; https://doi.org/10.1172/jci.insight.128199DS1) used as an unbiased cohort. The median AXL expression in the testing cohort was used as the cutoff value in the validation cohort to stratify patients into AXL^{hi} or AXL^{lo} protein expression groups. Clinical and pathological characteristics of the testing and validation cohorts (Supplemental Table 1), as well as the distribution of AXL expression levels among the patients with NSCLC (Supplemental Table 2) were similar. Representative IHC stains of NSCLC sections in the 2 patient cohorts are shown in Supplemental Figure 1. No differences in age, NSCLC histological subtype, tumor size, nodal status, or tumor stage were observed between the AXL^{hi} and the AXL^{lo} patients in the validation cohort (Supplemental Table 3). Median cancer-specific survival (CSS) and disease-free survival (DFS) were significantly lower in AXL^{hi} patients (52.8 and 41.3 months, respectively) compared with AXL^{lo} patients (170.5 and 49.7 months, respectively; Figure 1, A and B).

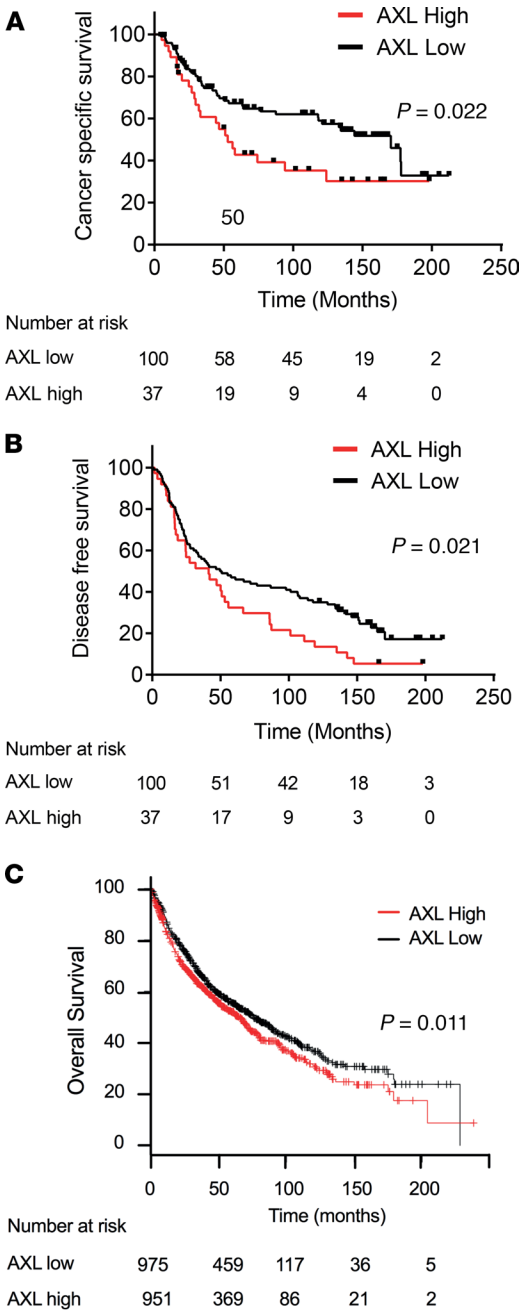

Figure 1. Correlation between AXL expression level in tumor tissue and patient outcome in cohorts of NSCLC patients. (**A** and **B**) Cancer-specific survival (CSS) and disease-free survival (DFS) in NSCLC patients with high and low AXL expression in tumor biopsies of 137 NSCLC patients. (**A**) Median CSS was 170.5 months (95% CI, 117.9 to >212.3) for patients with low AXL protein expression, as assessed by IHC (black line) vs. 52.8 months (95% CI, 29.6–123.9) for AXL^{hi} patients (red line) (P = 0.022, nonparametric log-rank test) in the validation cohort. (**B**) Median DFS was 49.7 months (95% CI, 30.3–101.3) for AXL^{lo} patients (black line) vs. 41.3 months (95% CI, 18.6–55.8) for AXL^{hi} patients (red line) (P = 0.021 nonparametric log-rank test) in the validation cohort. (**C**) High AXL mRNA expression was significantly associated with shorter overall survival (HR 1.18; 95% CI, 1.04–1.34; P = 0.011) in 1926 lung cancer patients analyzed with the gene expression survival analysis tool KM plotter. The median AXL expression was used as the cutoff in the Cox regression analysis.

Univariate Cox's proportional hazards regression analysis showed that AXL expression, age, and nodal status were prognostic factors for both CSS and DFS, while the multivariate analysis demonstrated that AXL expression, age, and nodal status were significantly associated with CSS. In addition, age and AXL expression were significantly associated with DFS (Supplemental Table 4). As an independent inquiry into the validity of our findings from the IHC analysis described above, we evaluated the prognostic significance of AXL expression in a cohort of 1926 lung cancer patients using the online gene expression survival analysis tool KM plotter (21). High AXL gene expression significantly correlated with shorter overall survival (OS; Figure 1C). Cumulatively, these data demonstrate that higher AXL expression is associated with poor prognosis of patients with NSCLC, supporting intervention strategies that specifically target AXL.

Enapotamab vedotin monotherapy is efficacious in an NSCLC mouse PDX clinical trial, and response is associated with AXL expression. To assess the antitumor activity of enapotamab vedotin (4 mg/kg) in preclinical NSCLC models in vivo, a mouse clinical trial (MCT) using PDXs was performed that consisted of a large and diverse collection of PDX models derived from patients with NSCLC (n = 61; Figure 2A). The collection comprised

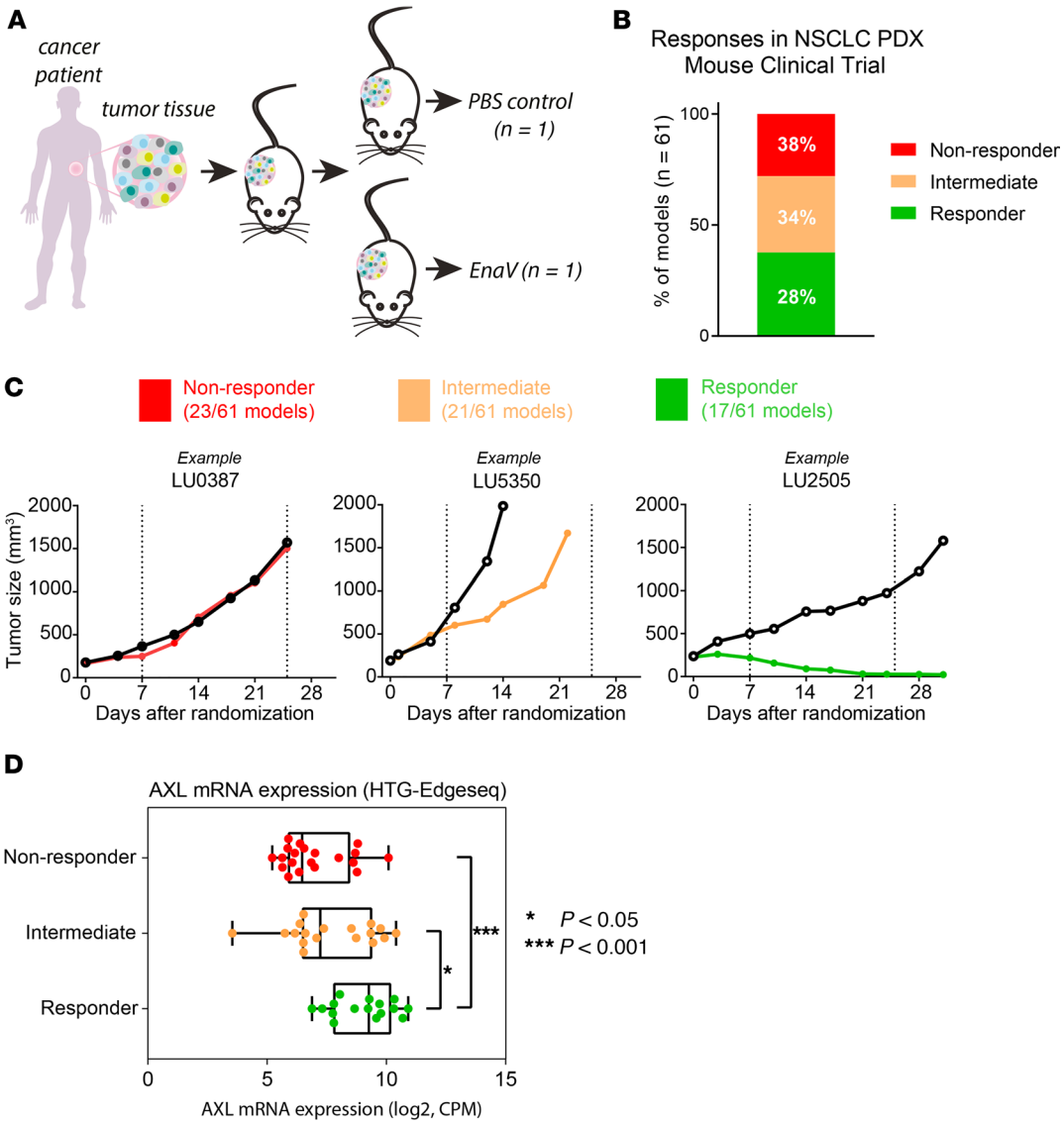

Figure 2. EnaV shows antitumor activity in an NSCLC mouse PDX clinical trial. (**A**) Schematic representation of PDX clinical trial design. Fragments of NSCLC patient-derived tumor cells were injected in 2 nude mice. Per PDX model, 1 mouse received a PBS injection (control), and the other mouse received treatment (EnaV, 4 mg/kg). (**B**) Antitumor activity of EnaV in an NSCLC mouse PDX clinical trial. Nonresponder (red), intermediate (orange), and responder (green) PDX models are indicated as percentage of a total of 61 PDX models tested. (**C**) Examples of each response category. Left plot: responder; middle plot: intermediate; right plot: nonresponder. Nonresponders are defined as models with a Δtreatment group/Δcontrol group (T/ΔC) ratio more than 70%, intermediates as models with ΔT/ΔC ratio between 10% and 70%, and responders as models with ΔT/ΔC ratio more than 10% after EnaV treatment. (**D**) AXL mRNA expression in responder, intermediate, and nonresponder NSCLC PDX models included in the mouse clinical trial as determined by HTG EdgeSeq. The box plots depict the minimum and maximum values (whiskers), the upper and lower quartiles, and the median. The length of the box represents the interquartile range. Statistically significant differences between groups determined by Mann-Whitney *U* test; $^{*}P < 0.05$, and $^{***}P = 0.0001$.

models of both adenocarcinoma and squamous cell carcinoma histology (19/61 and 22/61, respectively) and included predominantly *EGFR*–wild-type NSCLC (54/61) models, about a third of which (20 models) had a *KRAS* mutation (Supplemental Figure 2A). Seven of the 61 models harbored EGFR mutations that would qualify for EGFRi treatment in the clinic. Based on the change in tumor volume in an enapotamab vedotin–treated animal compared with a PBS-treated control animal, PDX models were classified as responder (tumor stasis or tumor regression in the enapotamab vedotin–treated animal) or nonresponder (tumor outgrowth comparable between enapotamab vedotin– and PBS-treated animals). Models that did not fall into either category were classified as intermediate. Seventeen models (28%) were categorized as responder, 21 (34%) as intermediate, and 23 (38%) as nonresponder (Figure 2B). Examples of the different response categories are shown in Figure 2C. To determine whether enapotamab vedotin treatment efficacy was associated with AXL

Table 1. EnaV shows dose-dependent antitumor activity in expanded NSCLC CDX and PDX models in vivo

	Model	*EGFR* mutation	AXL H-score	Efficacy (2 mg/kg)	Efficacy (4 mg/kg)
CDX	LCLC-103H[A,B]	WT	121	growth inhibition	complete regression
PDX	LXFA526[C]	WT	305	growth inhibition	complete regression
PDX	LU0395[D]	WT	117	regression	regression
PDX	LU2511[D]	WT	142	no effect	growth inhibition
PDX	LXFE772[C]	WT	101	no effect	no effect
PDX	LXFA677[C]	WT	183	growth inhibition	regression
PDX	LXFA677_R[C,E]	WT	248	complete regression	complete regression
PDX	LU1868[D]	L858R/T790M	104	growth inhibition	regression
PDX	LU0858[D]	L858R	141	no effect	growth inhibition
PDX	LCx-MR007[F]	L858R(/T790M loss)	n.d.	growth inhibition	regression

NSCLC CDX and PDX models (n = 7–10 mice per group) were treated with either 2 or 4 mg/kg (except for LCLC-103H, which was tested at 0.5 and 1.0 mg/kg). *EGFR* status of each model is indicated as wild-type (WT) or designated by its activating mutation (L858R and/or T790M). All models were *KRAS* wild-type; *KRAS* status of LCx-MR007 is unknown. [A]Model tested in-house. [B]Doses tested were 0.5 and 1 mg/kg; see Figure 3. [C]Model tested at Oncotest; see Figures 3 (LXFE772) and 4 (LXFA677/LXFA677_R; LXFA526) as previously published (20). [D]Model tested at Crown Bioscience; see Figures 3 (LU0395; LU2511) and 5 (LU1868; LU0858). [E]Erlotinib-resistant model derived from LXFA677 (24); see Figure 4. [F]Model tested at XenTech; see Figure 6. H-score, semiquantitative IHC assessment, which takes into consideration the staining intensity together with the percentage of cells staining positive; n.d., not determined.

expression in the PDX models, AXL mRNA expression was determined in untreated control tumors (available for 54/61 models). As shown in Figure 2D, AXL mRNA expression was significantly higher in PDX models that responded to enapotamab vedotin treatment (R models) compared to nonresponder PDX models (NR models), indicating a positive association between AXL expression and potent antitumor activity in vivo. The ethnic and histological backgrounds of the 17 PDX models responding to enapotamab vedotin treatment and the starting set of 61 models were similar, while *KRAS* mutations were slightly overrepresented in the models responding to enapotamab vedotin, and 2 models had an *EGFR* mutation (Supplemental Figure 2B).

Enapotamab vedotin shows in vivo antitumor activity in NSCLC cell line–derived xenograft and PDX models. The in vivo antitumor activity of enapotamab vedotin was confirmed in a panel of AXL-expressing NSCLC PDX or cell line–derived xenograft (CDX) models using 7–10 mice per group. AXL expression in these models was demonstrated by IHC (data not shown). Enapotamab vedotin induced antitumor activity in 9/10 models, including 3 *EGFR*-mutant models (Table 1, Figure 3, and Figure 4). Generally, more profound antitumor activity was observed at a dose of 4 mg/kg compared with 2 mg/kg. Complete tumor regression upon treatment with enapotamab vedotin was observed in CDX model LCLC-103H at a dose of 1 mg/kg (Figure 3A), while tumor regression was observed in PDX model LU0395 (Figure 3B) at doses of 2 and 4 mg/kg. Enapotamab vedotin (4 mg/kg) induced growth inhibition in PDX model LU2511 (Figure 3C), while it had no effect in PDX model LXFE772 (Figure 3D). Tumor sizes of enapotamab vedotin–treated groups were compared to those of a control group on the last day that both groups were intact, but no later than day 25 after randomization, because pharmacokinetic (PK) studies indicated all administered drug was cleared by day 25 (data not shown). This revealed a statistically significant reduction in tumor size in enapotamab vedotin–treated animals in CDX model LCLC-103H and PDX models LU0395 and LU2511 (Figure 3, E–G), while no statistically significant differences between groups were observed in PDX model LXFE772 (Figure 3H). As evident from these data, antibody-mediated targeting of the MMAE payload to AXL-expressing tumor cells resulted in potent antitumor activity in most NSCLC PDX models tested, implicating enapotamab vedotin monotherapy as a promising therapeutic approach in this indication.

Enapotamab vedotin shows antitumor activity in EGFRi-resistant NSCLC PDX models in vivo. Because AXL upregulation has been described to be a common acquired resistance mechanism upon EGFRi treatment in both preclinical and clinical studies (8, 9, 22, 23), we examined the effect of enapotamab vedotin in EGFRi-resistant models. The PDX model LXFA677, which is another *EGFR*–wild-type NSCLC model, albeit driven by EGFR activation, was rendered resistant against EGFRi by continuous in vivo exposure to gefitinib (24). The EGFRi-resistant LXFA677_R model displayed a relative enrichment of AXL^{hi}-expressing cancer cells compared with the parental PDX model LXFA677 (Figure 4, A and B). As expected, outgrowth of parental LXFA677 tumors in nude mice was inhibited by

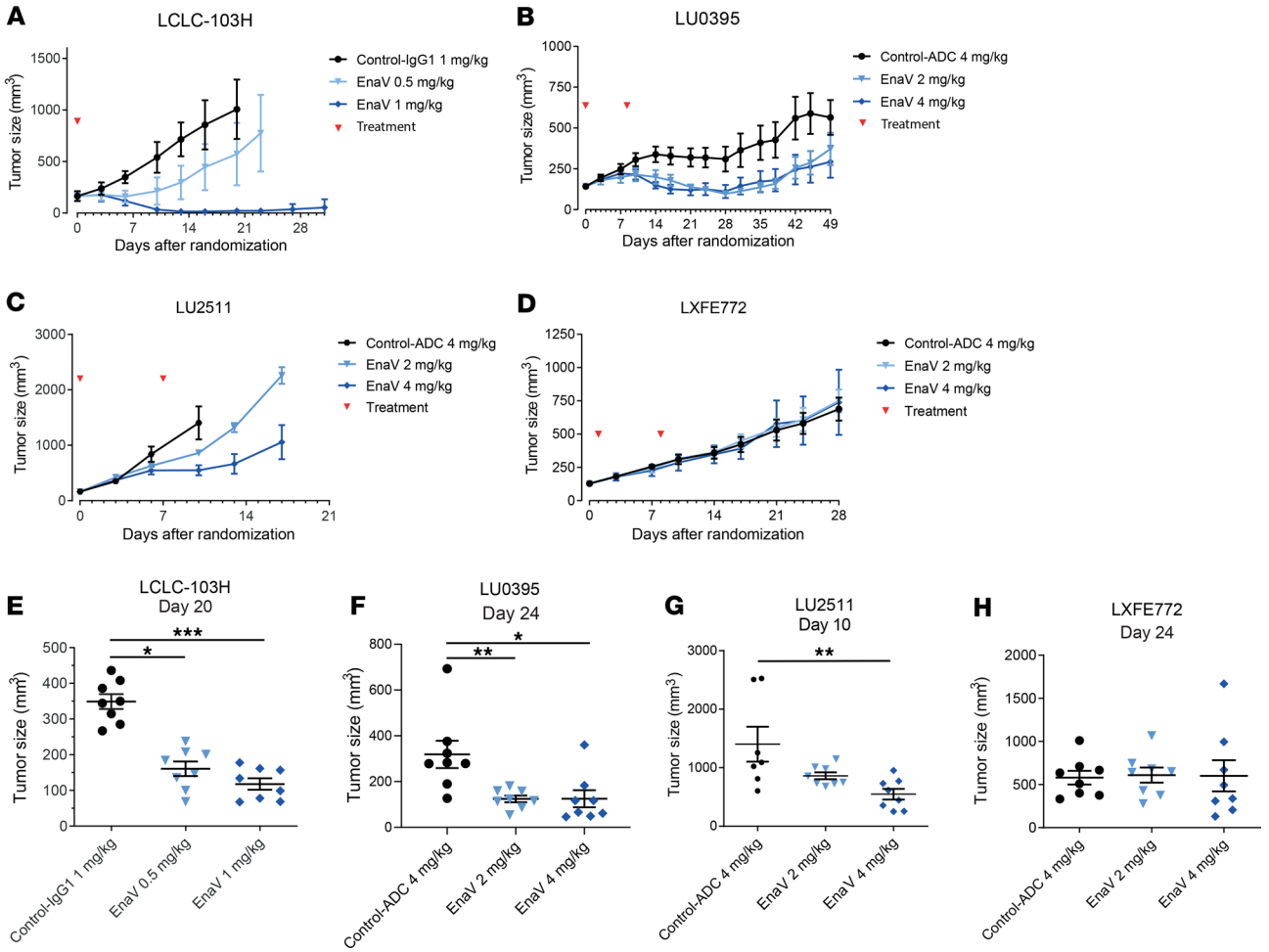

Figure 3. Dose-dependent tumor growth regression or inhibition induced by enapotamab vedotin in expanded NSCLC CDX and PDX models in vivo. Tumor growth curves of NSCLC CDX model LCLC-103H (**A**) and PDX models LU0395 (**B**), LU2511 (**C**), and LXFE772 (**D**), presented as mean tumor sizes of 7–10 mice per group. Mean tumor sizes are displayed up to the day the first mouse of a group was sacrificed. Days of EnaV or isotype-ADC treatment are indicated with red arrowheads. Statistical analysis (Mann-Whitney *U* test + Bonferroni's post hoc test; $^{*}P \leq 0.05$, $^{**}P \leq 0.01$, and $^{***}P < 0.001$) was performed on the last day that both groups were intact, but no later than day 25 after randomization, because PK studies indicated all administered drug was cleared by day 25 (data not shown), to identify significant differences in tumor sizes between groups. (**E**) Tumor sizes in CDX model LCLC-103H, compared on day 20 after randomization. (**F**) Tumor sizes in PDX model LU0395, compared on day 24 after randomization. (**G**) Tumor sizes in PDX model LU2511, compared on day 10 after randomization. (**H**) Tumor sizes in PDX model LXFE772, compared on day 24 after randomization.

erlotinib treatment, while LXFA677_R did not respond to erlotinib (Figure 4, C and D). Treatment with enapotamab vedotin resulted in inhibition of tumor growth in LXF677, which was statistically significant at a dose of 4 mg/kg but not at 2 mg/kg. In the LXFA677_R model, both doses of enapotamab vedotin induced complete and sustained tumor regression (Figure 4, E and F). These data indicate that increased AXL expression upon acquisition of EGFRi resistance renders NSCLC tumors more sensitive to enapotamab vedotin treatment, because we found a relative enrichment of AXL 3+ (high expressing) cancer cells in the LXFA677_R model rendered resistant under continuous EGFRi treatment in vivo compared with the sensitive parental LXFA677 PDX.

To study the in vivo efficacy of enapotamab vedotin in further detail in the *EGFR*-mutant segment, the activity of enapotamab vedotin as a monotherapy, as well as in combination, was investigated in 2 PDX models with clinically relevant activating *EGFR* mutations and clinical resistance to the EGFRi erlotinib. The LU1868 model has both the L858R and T790M mutations, while the LU0858 model has the L858R mutation only. Single-agent enapotamab vedotin treatment induced growth inhibition (at 2 mg/kg in LU1868; at 4 mg/kg in LU0858) or tumor regression (at 4 mg/kg in LU1868), while both models were confirmed to be insensitive to treatment with erlotinib as a single agent as well as the isotype-ADC IgG1-b12-vcMMAE (control-ADC; Figure 5, A–D). Comparison of the median tumor sizes

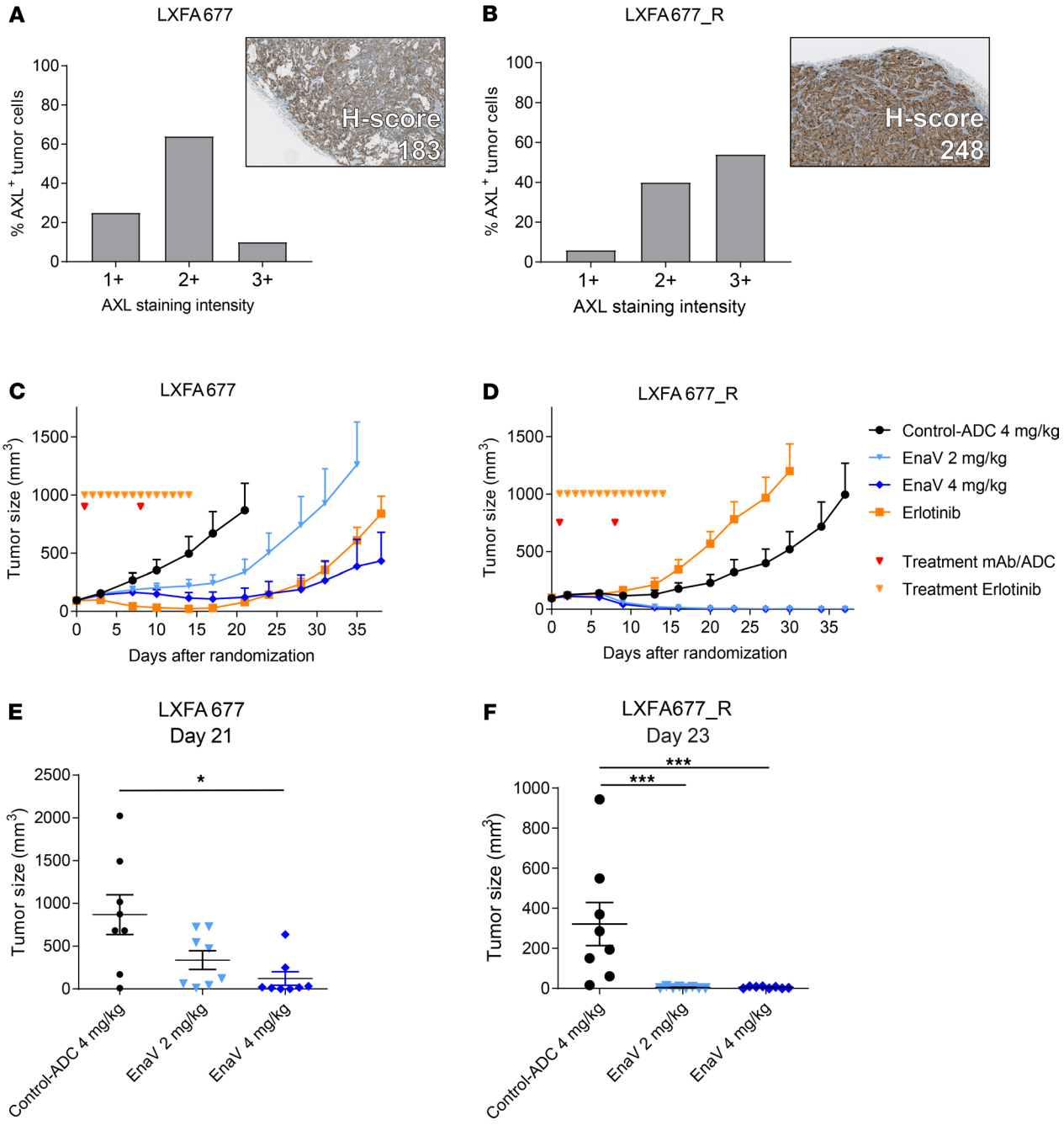

Figure 4. Increased sensitivity to EnaV treatment of EGFR-driven NSCLC PDX model LXFA677 upon acquiring EGFRi resistance. (**A** and **B**) Percentage of AXL-expressing parental LXFA677 cells, subdivided into percentage of low (1+), intermediate (2+), and strong (3+) staining cells of parental (**A**) and EGFRi-resistant (**B**) LXFA677 PDX models. Insert: representative cropped image of staining and calculated H-score for parental (**A**) and EGFRi-resistant (**B**) LXFA677 PDX models. (**C** and **D**) Tumor growth curves of parental (**C**) and EGFRi-resistant (**D**) LXFA677 PDX models, treated with EnaV (2 and 4 mg/kg), isotype-ADC, or erlotinib only. Red arrowheads indicate days of EnaV treatment; black arrowheads indicate days of erlotinib treatment. Tumor sizes are presented as mean tumor size of each group of mice (n = 8 per group) up to the day the first mouse of a group was sacrificed. (**E** and **F**) Statistical analysis (Mann-Whitney U test + Bonferroni's post hoc test; P values: $^{*}P < 0.05$, and $^{***}P \leq 0.001$) was performed on the last day that both groups were intact, but no later than day 25 after randomization, because PK studies indicated all administered drug was cleared by day 25 (data not shown), to identify significant differences in tumor sizes between groups. (**E**) Tumor sizes in parental model LXFA677, compared on day 21 after randomization. (**F**) Tumor sizes in EGFRi-resistant model LXFA677_R, compared on day 23 after randomization.

revealed a significant decrease in tumor size in mice treated with 4 mg/kg enapotamab vedotin in both models (Figure 5, C and E). Addition of erlotinib to enapotamab vedotin treatment had no significant effect on tumor growth of either PDX model compared to treatment with enapotamab vedotin alone (Figure 5, D, F, and G). However, both the enapotamab vedotin only and enapotamab vedotin plus

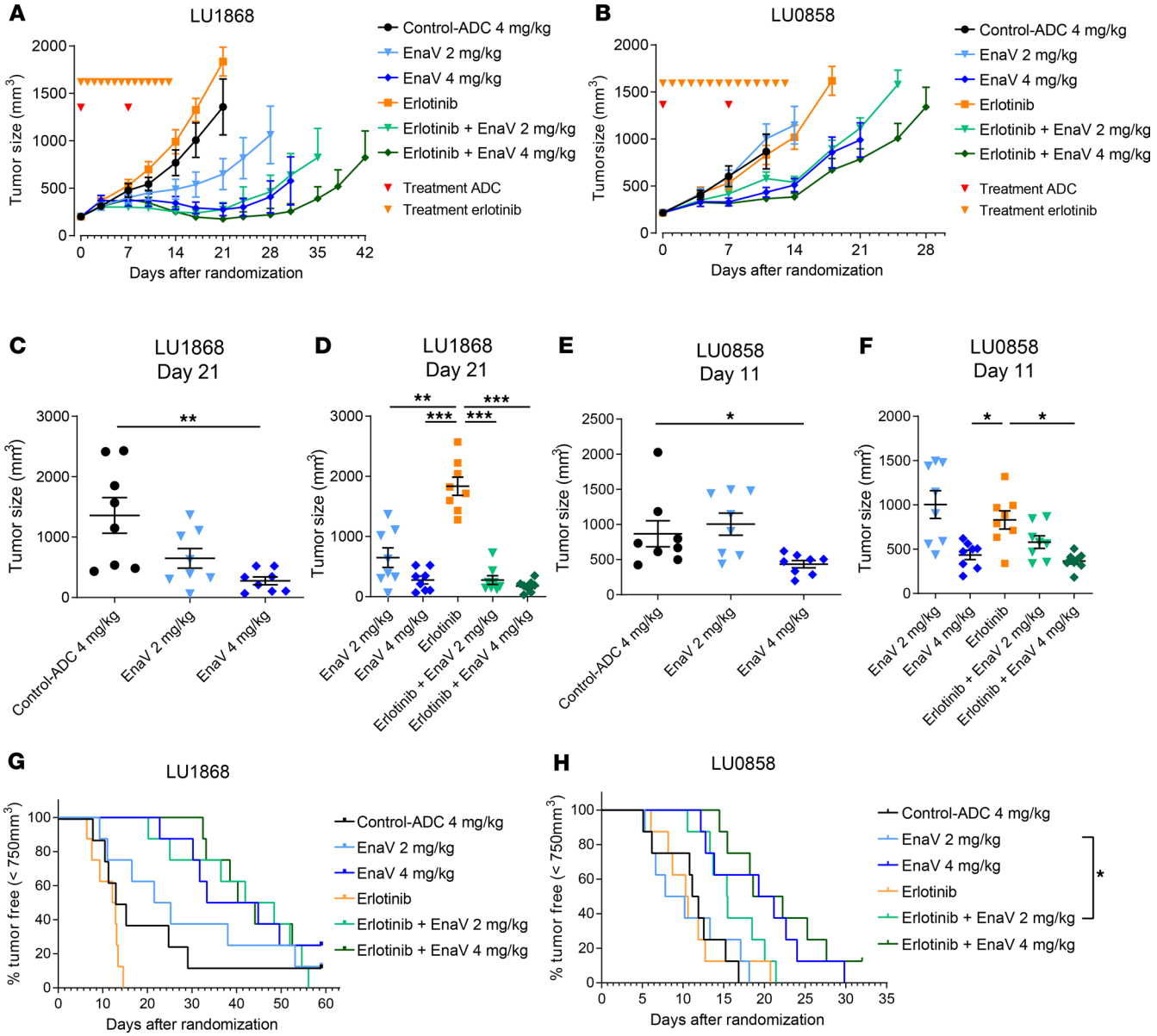

Figure 5. EnaV treatment overcomes resistance to EGFR inhibitors in vivo. (**A**) Tumor growth curves of the EGFR-mutant NSCLC PDX model LU1868 upon treatment with EnaV (2 mg/kg or 4 mg/kg) or erlotinib or combinations as indicated. Mean tumor sizes are displayed for each group (n = 8 per group) up to the day the first mouse of a group was sacrificed. Days of EnaV or isotype-ADC treatment indicated with red arrowheads; days of erlotinib treatment indicated with orange arrowheads. (**B**) Same as **A** for EGFR-mutant NSCLC PDX model LU0858. (**C–F**) Statistical analysis (Mann-Whitney U test + Bonferroni's post hoc test; P values: $^*P < 0.05$, $^{**}P \leq 0.01$, and $^{***}P \leq 0.001$) was performed on the last day that both groups were intact, but no later than day 25 after randomization, because PK studies indicated all administered drug was cleared by day 25 (data not shown), to identify significant differences in tumor sizes between groups. (**C** and **D**) Tumor sizes in the PDX model LU1868, compared on day 21 after randomization. (**E** and **F**) Tumor sizes in PDX model LU0858, compared on day 11 after randomization. (**G** and **H**) Combination therapy in EGFR-mutant, erlotinib-resistant NSCLC PDX models in vivo. Kaplan-Meier plots of NSCLC PDX model LU1868 (**G**) and LU0858 (**H**) after treatment with EnaV only (2 mg/kg or 4 mg/kg), erlotinib only, or combinations as indicated. Mice were considered tumor progression–free until a cutoff tumor size of 750 mm^3 was reached. Statistically significant differences determined by Mantel-Cox analysis, $^*P < 0.05$.

erlotinib combination treatment groups showed significantly smaller tumor sizes than groups of mice treated with erlotinib only (Figure 5, D and F), with the exception of the enapotamab vedotin–treated mice (2 mg/kg) in model LU0858.

In addition, a combination of enapotamab vedotin (2 mg/kg) and erlotinib significantly prolonged progression-free survival (defined as a tumor size < 750 mm^3) compared with enapotamab vedotin (2 mg/kg) alone in PDX model LU0858 (Figure 5H). Together, these results show preclinical antitumor activity of enapotamab vedotin against EGFRi-resistant AXL-expressing NSCLC models.

Table 2. Acquired resistance of EGFR-mutant NSCLC cells to EGFR inhibitors results in enhanced AXL expression and is associated with increased sensitivity to EnaV

Model	EGFR mutation	AXL molecules/cell[A]	Erlotinib sensitivity[B]	Osimertinib sensitivity[B]	EnaV sensitivity[C]	AXL-specific cytotoxicity at 1 μg/mL[D]
HCC827 parental	Δexon19	BLQ–4200	+[E]	n.d.	–	**0**
HCC-827-ER20		57,000–73,000	–[E]	n.d.	+	**60.0 ± 5.7**
HCC-827-ER30		8000–38,000	–[E]	n.d.	+	**54.0 ± 14.5**
PC9 parental	Δexon19	8000–24,000	+	+	–	**14.9 ± 23.4**
PC9-ER8		38,000–72,000	–	+	+	**66.3 ± 5.1**
PC9-OR1		54,000–71,000	–	–	+	**74.2 ± 8.1**
H1975 parental	L858R/T790M	9000–12,000	–	+	–	**0**
H1975-OR2		36,000–59,000	–	–	+	**97.2 ± 0.5**
H1650 parental	Δexon19	3000–15,000	+/–[F]	+/–[F]	–	**3.1 ± 5.2**
H1650-ER16		13,000–62,000	–	–	+/–[G]	**38.8 ± 25.2**
H1650-OR2		51,000	–	–	+/–[G]	**27.3 ± 17.2**
HCC4006 parental	Δexon19	BLQ–11,000	+	+	+/–[G]	**23.3 ± 29.3**
HCC4006-ER0.3		35,000–55,000	–	–	–	**0.9 ± 1.5**
HCC4006-OR0.1		25,000–82,000	–	–	+	**33.9 ± 20.2**

Summary of results from 5 NSCLC cell lines and their EGFRi-resistant derivatives treated with erlotinib or osimertinib or EnaV in vitro. Naming of cell lines: ER: erlotinib resistant; OR: osimertinib resistant, followed by a number denoting micromolar of drug concentration the cell line was resistant to. Cell line sensitivity to erlotinib, osimeritinib, or EnaV indicated with +. [A]Determined by quantitative FACS (Qifi) analysis, range determined in at least 2 experiments, performed in duplicate (Figure 7). [B]Sensitivity to erlotinib or osimertinib is defined as a >25% reduction in viability at a concentration of 0.1 μM. [C]Sensitivity to AXL-ADC is defined as a >25 % reduction in viability at a concentration of 1 μg/mL, relative to the control ADC (IgG1-b12-MMAE). [D]AXL-specific cytotoxicity relative to the control-ADC; average of at least 2 experiments, performed in duplicate or triplicate. [E]EGFR inhibitors erlotinib, gefitinib, and afatinib tested on this cell line showed similar results. [F]Viability was reduced by approximately 25% relative to no erlotinib treatment. [G]Variability in AXL-specific cytotoxicity relative to the control-ADC across experiments: does not consistently meet the 25% definition. BLQ, below lowest level of quantitation (2100 molecules/cell); n.d., not determined.

Acquired resistance of EGFR-mutant NSCLC cell lines to EGFRi results in enhanced AXL expression and is associated with increased sensitivity to enapotamab vedotin. Acquired resistance against first- or second-generation EGFRi, such as erlotinib or gefitinib, is often induced by a secondary mutation, T790M in exon 20 (17). The third-generation EGFRi osimertinib, which also inhibits EGFR kinase activity in the presence of the T790M mutation, was recently approved by the FDA for first-line treatment of metastatic NSCLC with activating EGFR mutations (25). Unfortunately, acquired resistance against osimertinib is a growing clinical challenge, and alternative treatment options in *EGFR*-mutant NSCLC are needed (26). To mimic clinical resistance to EGFRi, we generated 5 erlotinib- and/or osimertinib-resistant NSCLC cell lines by continuous exposure to increasing concentrations of either erlotinib or osimertinib in vitro. Upon acquiring resistance to EGFRi, the cell lines were characterized for AXL expression and sensitivity to enapotamab vedotin and compared with their parental cell lines (Table 2). NSCLC cell line HCC827 harbors the *EGFR* exon 19 deletion (delE746-750) and was previously described by Zhang et al. (2012) as upregulating AXL expression upon acquiring resistance to erlotinib (9). Likewise, we generated an erlotinib-resistant HCC827 cell line (HCC827-ER20) (Figure 7A) and noted enhanced AXL expression in the HCC827-ER20 cell line compared with the erlotinib-sensitive parental HCC827 cell line (Figure 7, B and C). Although the parental HCC827 cell line was highly sensitive to the first- and second-generation *EGFR* inhibitors erlotinib, gefitinib, and afatinib (Supplemental Figure 4), HCC827-ER20 cells showed cross-resistance to treatment with these inhibitors (Figure 7A). Consistent with upregulated AXL expression, HCC827-ER20 cells were shown to be sensitive to enapotamab vedotin exposure in vitro (Figure 7D), while the parental cell line was not. This demonstrates that the enhanced expression of AXL seen in EGFRi-resistant cells is sufficient to allow targeting with enapotamab vedotin.

Similar data were obtained with 4 other *EGFR*-mutant cell lines for which EGFRi-resistant derivatives were generated. The parental PC9, H1650, and HCC4006 NSCLC cell lines were sensitive to both erlotinib and osimertinib, while H1975, which harbors the T790M mutation, was sensitive to osimertinib only, as expected (Table 2 and Figure 7E). Acquisition of EGFRi resistance was associated with

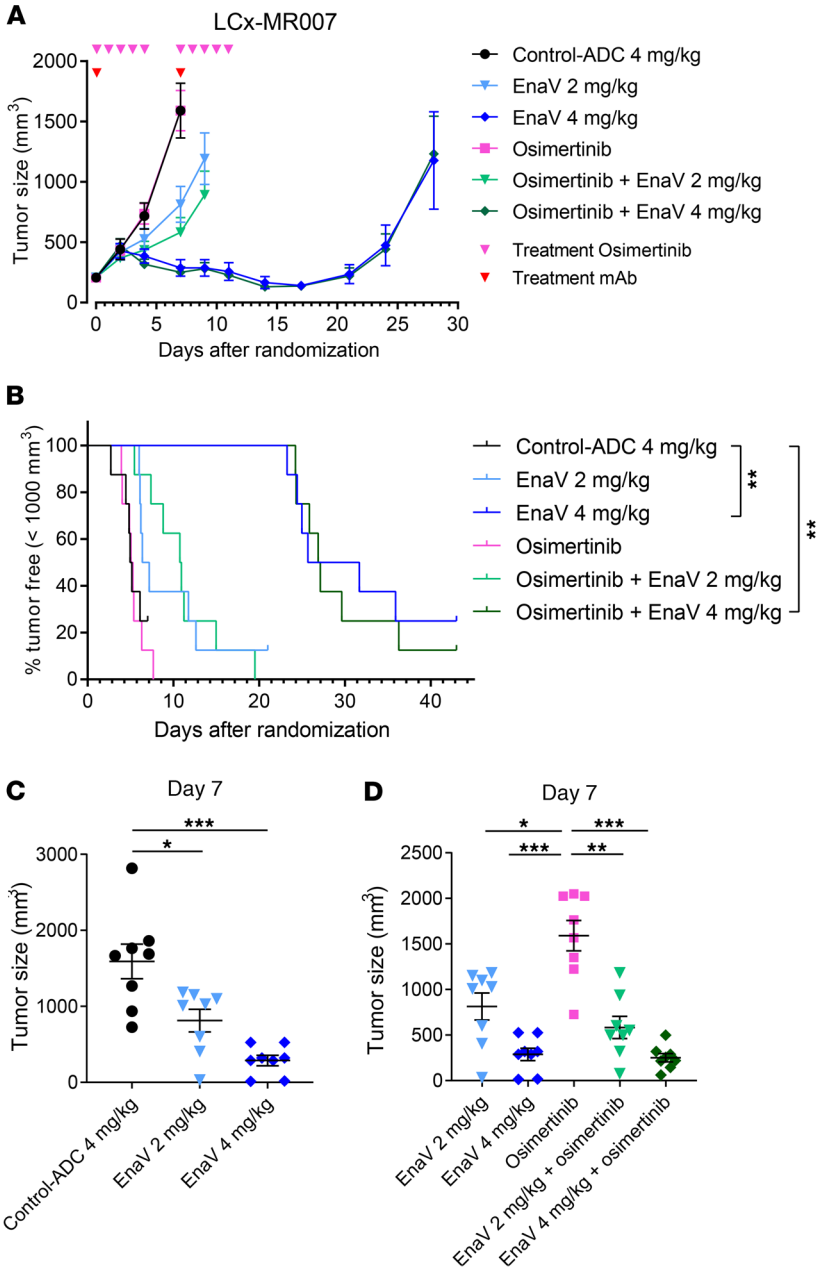

Figure 6. Efficacy of EnaV monotherapy and combination therapy in an osimertinib-resistant NSCLC PDX model. (**A**) Tumor growth curves of the osimertinib-resistant NSCLC PDX model LCx-MR007 upon treatment with EnaV (2 mg/kg or 4 mg/kg) or osimertinib or combinations as indicated. Mean tumor sizes are displayed for each group (n = 8 per group) up to the day the first mouse of a group was sacrificed. Days of EnaV or isotype-ADC treatment indicated with red arrowheads; days of osimertinib treatment indicated with pink arrowheads. (**B**) Kaplan-Meier survival plot of the osimertinib-resistant PDX model LCx-MR007 treated with EnaV (2 mg/kg or 4 mg/kg), osimertinib, or combinations as indicated. (**C** and **D**) Tumor sizes compared on day 7 after randomization. Statistical analysis (Mann-Whitney U test + Bonferroni's post hoc test; P values: $^{*}P \le 0.05$, $^{**}P \le 0.01$, and $^{***}P \le 0.001$) was performed on the last day that both groups were intact, but no later than day 25 after randomization, because PK studies indicated all administered drug was cleared by day 25 (data not shown), to identify significant differences in tumor sizes between groups.

enhanced AXL expression in all the resistant cell lines (Figure 7F). Illustrating the potency of enapotamab vedotin, strong cytotoxicity of osimertinib-resistant H1975-OR2 was induced by enapotamab vedotin, while the enapotamab vedotin effect on cytotoxicity in the parental cell line H1975 was negligible and not different from the control-ADC (Figure 7G). Similarly, enhanced sensitivity to enapotamab vedotin was observed in the resistant derivatives of the PC9, H1650, and HCC4006 cell lines, particularly of osimertinib-resistant derivatives (Supplemental Figure 5). Of note, high AXL expression and sensitivity to enapotamab vedotin exposure were retained even if the osimertinib-resistant cell lines were cultured in the absence of osimertinib for up to 3 weeks (Supplemental Figure 6), which suggests that the acquired resistance phenotype is also maintained in the absence of the drug. Interestingly, despite enhanced AXL expression, the HCC4006-ER0.3 cell line was insensitive to enapotamab vedotin exposure. To evaluate the underlying cause of this insensitivity, we determined sensitivity of each of the cell line variants to free MMAE. As shown in Supplemental Figure 7, parental and osimertinib-resistant cell lines showed similar, strong sensitivity to free MMAE. In contrast, HCC4006-ER0.3 showed greatly diminished sensitivity to free MMAE, reflecting reduced enapotamab vedotin sensitivity of this cell line.

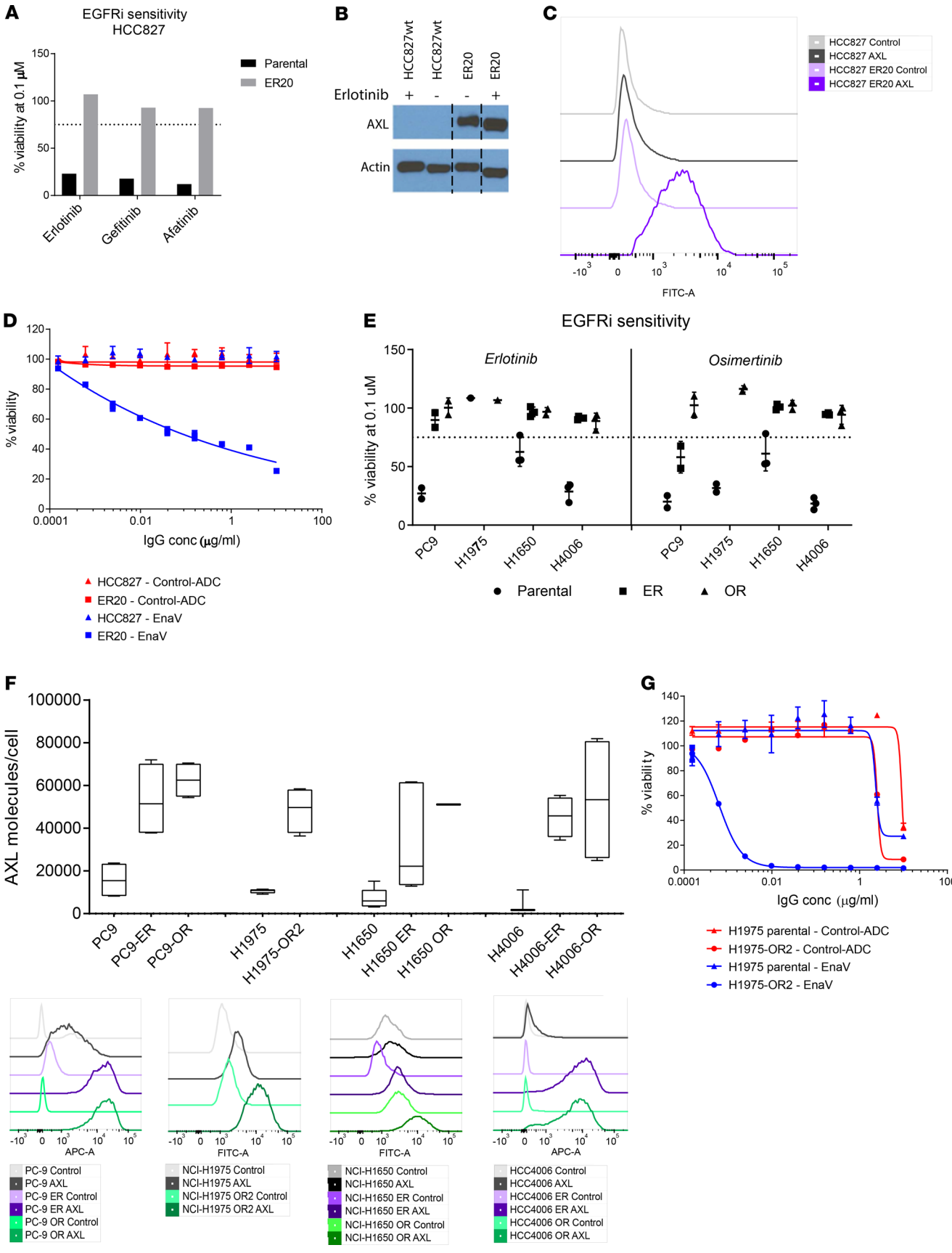
A
EGFRi sensitivity
HCC827
% viability at 0.1 μM
Parental
ER20
Erlotinib
Gefitinib
Afatinib
B
HCC827wt
HCC827wt
ER20
ER20
Erlotinib + - - +
AXL
Actin
C
HCC827 Control
HCC827 AXL
HCC827 ER20 Control
HCC827 ER20 AXL
FITC-A
D
% viability
IgG conc (μg/ml)
HCC827 - Control-ADC
ER20 - Control-ADC
HCC827 - EnaV
ER20 - EnaV
E
EGFRi sensitivity
Erlotinib
Osimertinib
% viability at 0.1 uM
PC9
H1975
H1650
H4006
Parental
ER
OR
F
AXL molecules/cell
PC9
PC9-ER
PC9-OR
H1975
H1975-OR2
H1650
H1650 ER
H1650 OR
H4006
H4006-ER
H4006-OR
APC-A
FITC-A
PC-9 Control
PC-9 AXL
PC-9 ER Control
PC-9 ER AXL
PC-9 OR Control
PC-9 OR AXL
NCI-H1975 Control
NCI-H1975 AXL
NCI-H1975 OR2 Control
NCI-H1975 OR2 AXL
NCI-H1650 Control
NCI-H1650 AXL
NCI-H1650 ER Control
NCI-H1650 ER AXL
NCI-H1650 OR Control
NCI-H1650 OR AXL
HCC4006 Control
HCC4006 AXL
HCC4006 ER Control
HCC4006 ER AXL
HCC4006 OR Control
HCC4006 OR AXL
G
% viability
IgG conc (μg/ml)
H1975 parental - Control-ADC
H1975-OR2 - Control-ADC
H1975 parental - EnaV
H1975-OR2 - EnaV

Figure 7. Increased AXL expression and sensitivity to EnaV in a panel of *EGFR*-mutant NSCLC cell lines upon acquired resistance to EGFR inhibitors in vitro. (**A**) Cell viability of the NSCLC parental and erlotinib-resistant (ER20) HCC827 cell line after exposure to erlotinib, gefitinib, or afatinib. (**B**) Detection of AXL protein on parental and erlotinib-resistant HCC827 NSCLC cells as determined by Western blot. A full, uncut, and unedited version of the blot is provided in Supplemental Figure 3. (**C**) Histogram representing AXL protein expression on parental and erlotinib-resistant HCC827 NSCLC cells as determined by flow cytometry. (**D**) Cell viability (in vitro cytotoxicity) of parental and erlotinib-resistant HCC827 NSCLC cells after exposure to EnaV or isotype-ADC at the indicated concentrations. (**E**) Cell viability of NSCLC cell lines PC9, H1975, H1650, and HCC4006 and resistant derivatives (ER/OR) upon exposure to 0.1 μM erlotinib (left half of graph) or osimertinib (right half of graph). Percentage of cell viability was calculated relative to the percentage of cells alive after exposure to isotype-ADC at the same concentration. (**F**) Expression of AXL on NSCLC cell lines and resistant derivatives as determined by flow cytometry. The box plots depict the minimum and maximum values (whiskers), the upper and lower quartiles, and the median. The length of the box represents the interquartile range. (**G**) Cell viability of parental NSCLC cell lines H1975 and osimertinib-resistant derivative H1975-OR2 (considered osimertinib resistant at 2 μM osimertinib concentration) upon exposure to indicated concentrations of EnaV or isotype-ADC. Viability was calculated as follows: % viability = (luminescence sample of interest – luminescence STAU) / (average luminescence of control vehicle treated – luminescence STAU), with STAU representing 1 μM staurosporin for 100% cell killing.

To further evaluate the kinetics of AXL induction, we studied the expression of AXL over the course of EGFRi treatment using 2 AXL^{lo} or AXL^{-} NSCLC cell lines. No acute induction of AXL was observed in the AXL^{lo} cell line H1975 after 72 hours of osimertinib treatment, whereas enhanced AXL expression was observed after 3–4 months of osimertinib treatment (Supplemental Figure 8, A–D). Similar AXL induction upon erlotinib or osimertinib exposure for 3–5 months was observed in the AXL^{-} HCC4006 cell line (Supplemental Figure 8, E and F).

Enapotamab vedotin induces potent antitumor activity in an osimertinib-resistant NSCLC PDX model in vivo. Finally, we assessed the in vivo antitumor activity of enapotamab vedotin in the AXL-expressing PDX model LCx-MR007, derived from a patient with NSCLC who acquired resistance to osimertinib in the clinic (27, 28). Although osimertinib had no effect on tumor growth, tumor regression was observed in mice treated with enapotamab vedotin at a dose of 4 mg/kg (Figure 6A). Inhibition of tumor growth was achieved by treating mice with the 2 mg/kg dose of enapotamab vedotin. The progression-free survival of mice treated with 4 mg/kg enapotamab vedotin was significantly prolonged as compared with the group treated with the control-ADC (log-rank test; $P < 0.01$; Figure 6B). On day 7, the last day when all groups were intact, a statistically significant reduction in tumor size was observed in both the 2 mg/kg and 4 mg/kg enapotamab vedotin dose groups compared to the control-ADC (Figure 6C). Combining enapotamab vedotin treatment with osimertinib did not further enhance the antitumor effects, similar to what was observed for combined enapotamab vedotin and erlotinib treatment (Figure 5, A and B, and Figure 6D), although all enapotamab vedotin–treated groups, either alone or in combination with osimertinib, showed a significant reduction in median tumor size compared with mice treated with osimertinib only. Taken together, these results warrant further validation of enapotamab vedotin treatment in EGFRi-resistant NSCLC tumors, including tumors resistant to the recently approved EGFRi osimertinib.

Discussion

The market entry of targeted therapies more than a decade ago has revolutionized the treatment of NSCLC. More recently, immune checkpoint inhibitors, such as α–programmed cell death 1 (α–PD-1) and α–PD-1 ligand 1, have shown remarkable efficacy in *EGFR*–wild-type NSCLC (3, 29). Still, only a minority of patients derive long-term benefit from these therapies, emphasizing the need for novel treatment options across NSCLC subtypes. AXL may represent a valuable target because its expression was shown to be associated with increased invasiveness and EMT and resistance to multiple classes of therapeutics agents (30–32). These include inhibitors of the EGFR/MAPK pathway in various cancers, including NSCLC (8, 9, 20). In the current study, we present preclinical validation of the potential of enapotamab vedotin, an AXL-targeting ADC, to treat NSCLC. Enapotamab vedotin demonstrated strong cytotoxicity in vitro and antitumor activity in vivo in a variety of NSCLC PDX models, including both *EGFR*–wild-type and EGFRi-resistant, *EGFR*-mutant NSCLC tumors.

To confirm the prognostic potential of AXL in NSCLC, we examined AXL expression in primary tumors in 3 independent cohorts of patients with NSCLC. Our results showed that high expression of AXL was significantly correlated with a shorter CSS and DFS or OS. Our findings are supported by 3 other studies that also found a significant correlation between AXL expression and DFS and/or OS (33–35). Multivariate analyses to investigate whether the prognostic value of AXL expression was affected by underlying clinicopathological covariates were inconclusive in 1 study (34) or not performed (35). Thus, our study provides additional confirmation of the prognostic value of AXL expression in NSCLC progression and provides a rationale for targeting AXL.

AXL has been found to be relatively overexpressed in an *EGFR*–wild-type segment of NSCLC cell lines with an EMT-like gene signature, characterized by mesenchymal features and frequent KRAS mutations (8). In addition, AXL upregulation has been found to be associated with EMT and played an important role in the acquisition of erlotinib resistance in EGFRi-resistant NSCLC (9). Similarly, our previous work in melanoma showed that upregulation of AXL is associated with acquisition of resistance against inhibitors of the downstream MAPK pathway (9, 20). We have not evaluated the association between AXL expression and the presence of specific molecular alterations also known to be associated with resistance to second- and third-generation EGFRi, such as MET amplification, PIK3CA, EGFR C797S, KRAS, erb-b2 RTK2, ephrin type-A receptor 2, fibroblast growth factor receptor, and Mer, because this has been evaluated by others (15–19).

The data presented here demonstrate distinct preclinical therapeutic activity of enapotamab vedotin in both the *EGFR*–wild-type as well as the *EGFR*-mutant segments of NSCLC. In an MCT, potent responses to enapotamab vedotin were associated with higher AXL expression. Tumor stasis or tumor regression were noted in almost 30% of NSCLC PDX models, representing diverse histological and mutational backgrounds. The distribution of ethnicity and histological subtypes was similar in the 17 models responding to enapotamab vedotin treatment and in the complete cohort of 61 models. Interestingly, *KRAS* mutations were more frequent in the models responding to enapotamab vedotin: about half of the responding models had a *KRAS* mutation, whereas about a third of the complete MCT panel was *KRAS* mutant. Out of the 7 *EGFR*-mutant models in the MCT panel, 2 models responded to enapotamab vedotin. Although these results represent small numbers and the prior treatment status of the models is not available, it is tempting to speculate that the responses depend on prior clinical treatment, either with chemotherapy in the *KRAS* segment and with EGFRi in the *EGFR*-mutant segment, that could induce targetable AXL expression levels. Signaling pathways downstream of AXL have been reported to induce EGFRi resistance via signals converging on the PI3K/Akt and MAPK pathways (36).

In addition to resistance to EGFRi, AXL overexpression has been associated with resistance to other targeted and chemotherapeutic agents in NSCLC, as recently reviewed (37). The evidence for this association is derived primarily from preclinical studies in vitro, where AXL upregulation was found in cell lines resistant to targeted agents such as PI3K inhibitors (8) or chemotherapeutics like paclitaxel, cisplatin, carboplatin, vincristine, or etoposide (38–40). Clinically, AXL expression has been associated with intrinsic resistance to checkpoint inhibitors in melanoma, where high AXL mRNA levels were found in the tumors of patients refractory to α–PD-1 treatment (11). Efforts are ongoing to further unravel the mechanisms that confer resistance to immune checkpoint inhibition, which include lack of (presentation of) tumor (neo-)antigens, the presence of immunosuppressive cells in the tumor microenvironment, and severe T cell exhaustion (41). AXL may be involved in some of these mechanisms because AXL is known to suppress the function of antigen-presenting cells (APCs) by dampening Toll-like receptor–induced responses (42, 43). Although these results require further confirmation, particularly in human tumors in vivo, they further support AXL as an attractive target in treatment-resistant NSCLC.

Similar to previous reports (9), we demonstrate that AXL expression was generally upregulated in NSCLC cell lines resistant to first-generation EGFRi. We show that this phenomenon also applies to osimertinib treatment resistance, as was recently reported by others (22, 44). Of interest, this third-generation EGFRi is now used as first-line treatment for NSCLC (25). Because of the relatively recent market entry of osimertinib, studies assessing AXL upregulation in osimertinib-resistant patients are still scarce and include analyses of genomic alterations only and not alterations of protein expression, such as AXL (26, 45–47). A retrospective study by Taniguchi et al. described IHC analysis performed on specimens from patients who were candidates for osimertinib treatment (44). Although this analysis concerned only a small sample size (n = 11) and evaluated tissues before treatment, the data did support higher AXL expression in tumors from patients with intrinsic resistance to osimertinib: the response rate was lower in patients with AXL expression of 3+ (67%) versus those with AXL 1+ or 2+ (weak and moderate, respectively) expression in tumors (88%), and a trend toward earlier relapse was seen in patients with AXL 3+ scores. Another study analyzing resistance mechanisms to another third-generation EGFRi (abivertinib) in tumor biopsies identified AXL amplification as a resistance mechanism in 1 of 23 paired patients' samples (48). Although we were not able to study clinical samples because of limited access to tissues from such studies, AXL expression is known to be associated with resistance to EGFRi in general, including osimertinib. In our study, AXL mediated cross-resistance between EGFRi in vitro, suggesting that AXL expression is a more general resistance mechanism than, e.g., T790M. In line with this, the data of Taniguchi et al., referenced above (44), suggest that intrinsic high AXL expression correlates with relative unresponsiveness to EGFRi treatment in general and osimertinib specifically.

The exact mechanisms behind the enhanced expression of AXL by NSCLC cells have not yet been elucidated. As we have shown in melanoma, AXL upregulation could be induced by 2 mechanisms: (a) enrichment of preexisting subpopulations of AXL-expressing cells in tumor specimens from treated patients and (b) acute transcriptional induction of AXL expression by drug treatment, including MEK inhibitors (20). The latter mechanism could be specific for MEK inhibitors, and not for EGFRi, because we did not observe acute induction in our studies. In the current study, we observed upregulation of AXL expression by NSCLC cell lines over months of EGFRi treatment, rather than acute induction of AXL expression. Whether the upregulation is due to de novo induction of AXL expression or enrichment of preexisting AXL^+ cells cannot be concluded from these data. However, the data on our LXFA677 PDX model support the notion that AXL-overexpressing tumors emerge via enrichment of rare AXL^{hi} cells over the course of therapy, because we found a relative enrichment of 3+ cancer cells in the LXFA677_R model that were rendered resistant under continuous EGFRi treatment in vivo compared with the sensitive parental LXFA677 PDX.

We observed that upregulation of AXL coincided with enhanced sensitivity to enapotamab vedotin in all cell lines tested, except derivative cell line HCC4006-ER, in which increased sensitivity to enapotamab vedotin treatment was not observed. This cell line was less sensitive to free MMAE than its parental and osimertinib-resistant counterparts. We have previously shown that increased expression of the multidrug resistance pump MDR1, which is known to extrude free MMAE, can lead to decreased MMAE sensitivity and resistance to enapotamab vedotin (20). Although not confirmed experimentally, this phenomenon may play a role in the case of HCC4006-ER as well.

The present study provides preclinical rationale for the clinical validation of enapotamab vedotin as a therapeutic agent in *EGFR*–wild-type and -mutant NSCLC patients, including those with (acquired) resistance to EGFRi. Acquired resistance of *EGFR*-mutant NSCLC cells to EGFRi, including the third-generation EGFRi osimertinib, resulted in enhanced AXL expression and increased sensitivity to enapotamab vedotin in vitro and in vivo. The clinical safety and preliminary activity of enapotamab vedotin is currently being assessed in a phase I/II clinical trial in a mixed population of solid tumors, including *EGFR*-mutant and *EGFR*–wild-type NSCLC (ClinicalTrials.gov identifier NCT02988817).

Methods

Cell culture and generation of EGFRi-resistant NSCLC cell lines. The HCC827, H1975, H1650, and HCC4006 NSCLC cell lines were purchased from the ATCC and PC9 NSCLC cells from ECACC (MilliporeSigma). Cells were cultured in RPMI1640 supplemented with 10% fetal bovine serum and 1% penicillin-streptomycin in a humidified atmosphere with 5% CO_2 at 37°C. These parental cell lines were all derived from lung adenocarcinomas featuring specific *EGFR* mutations and associated EGFRi sensitivities (49–53). To generate EGFRi-resistant derivative cell lines, parental cells were cultured in the presence of increasing concentrations of EGFRi. When cells adapted to a given dose of EGFRi, the concentration was raised by 50%–100% over 3–6 months, resulting in cell lines resistant to various EGFRi concentrations, as summarized in Table 2. Cell lines were maintained in culture medium supplemented with the designated concentration of erlotinib or osimertinib. The cell lines HCC827 and H1975 retained the same level of resistance when cultured without drugs (data not shown).

EGFRi. *EGFR* inhibitors (erlotinib, gefitinib, afatinib, and osimertinib [AZD9291]) were purchased from Selleck Chemicals, and stock solutions of 10 mM were prepared in DMSO.

Immunohistochemical staining of FFPE tissue microarrays. FFPE slides were freshly cut (at 4-μm slice thickness) from FFPE tissue microarray (TMA) blocks purchased from Biomax (testing cohort) or from a consecutive series of NSCLC surgical patients from Odense University Hospital (validation cohort; ref. 54). The validation TMA contained 1–4 cores from each of 137 NSCLC patients (2 cores from border areas and 2 from more central tumor areas). All patients had stage I–IIIA disease, and none had received any adjuvant/neoadjuvant chemo- or radiotherapy. Clinical data were assessed in accordance with a protocol approved by the Ethics Committee of Region Southern Denmark. Staining was performed on a VENTANA BenchMark Ultra (IHC Autostainer, Roche). Before staining, FFPE tissue slides were deparaffinized in 100% xylene (MilliporeSigma, 16446; 3 times, 5 minutes) and dehydrated in 96% ethanol (MilliporeSigma, 32294; 2 times, 5 minutes) at room temperature (RT). Thereafter, antigen retrieval was performed on the VENTANA autostainer by incubating slides in cell conditioning 1 buffer (VENTANA Medical Systems, Inc., Roche, 950-124) for 24 minutes and blocking for endogenous peroxidase using VENTANA BenchMark's default protocol.

AXL expression was determined by incubating tissue slides with 3 μg/mL rabbit polyclonal anti–human AXL antibody (sc-20741, Santa Cruz Biotechnology) in reaction buffer (Tris-based buffer solution at pH 7.6, 950-300, VENTANA Medical Systems, Inc., Roche) at 36°C for 32 minutes (VENTANA BenchMark, Roche). AXL-bound antibody was detected with an OptiView detection kit (poly–HRP-conjugated anti-mouse and anti-rabbit IgG; OptiView DAB IHC Detection Kit, 760-700, VENTANA Medical Systems, Inc., Roche). HRP was visualized with ChromoMap DAB (OptiView DAB IHC Detection Kit, 760-700, VENTANA Medical Systems, Inc., Roche); nuclei were counterstained with hematoxylin II (VENTANA Medical Systems, Inc., Roche, 790-2208) and Bluing reagent (VENTANA Medical Systems, Inc., Roche, 760-2037).

Validation of rabbit polyclonal antibody sc-20741 and evaluation in IHC analyses on FFPE tissue. The rabbit polyclonal anti-AXL antibody (Santa Cruz Biotechnology; sc-20741) was validated for research-grade IHC studies on FFPE tissues in several experiments (data not shown). In brief, the antibody bound specifically and in a concentration-dependent manner to permeabilized AXL-transfected human embryonic kidney 293 (HEK293) cells, but not to wild-type HEK293 cells (Life Technologies), as determined by flow cytometry. IHC staining of a microarray of FFPE pellets of several tumor cell lines also showed concentration-dependent binding, while the staining intensity corresponded with levels of AXL expression on the plasma membrane of these cell lines, as determined by the quantitative flow cytometry method described below. Finally, AXL IHC results were comparable with AXL mRNA in situ hybridization using RNAscope (ACD, Bio-Techne) with a human AXL–specific probe on FFPE slides of AXL-transfected HEK293 cells or AXL^+ tumor cell lines A431 and LCLC-103H (DSMZ), as well as on xenograft tissues from AXL^+ CDX or PDX models. IHC with sc-20741 and AXL-RNAscope revealed specific and similar cellular staining patterns across samples, while no signals were detected on AXL^- control cells (untransfected HEK293 cells).

Slide scanning and quantification of AXL staining intensity. All stained slides were digitized with an Axio Scan.Z1 (Zeiss) slide scanner at original magnification ×20, exported as .zvi (AxioScan) files, and subjected to quantitative image analysis with Definiens Tissue Studio software (version 4.1). For all tumor TMAs, a grid layout was generated to annotate each individual tumor tissue core. For each tissue core, the percentage of AXL^+ tumor cells (based on both membrane and cytoplasmic staining) and the AXL staining intensity (brown chromogen intensity) of individual tumor cells were quantified using a cell-based algorithm.

Tumor regions of interest (ROIs) for each NSCLC tissue core were identified on the basis of histopathological features by a trained and experienced technician. If deemed necessary, tumor ROI delineation was cross-validated by a certified pathologist. Tumor tissue cores were excluded from analysis when tissue morphology was of poor quality or when the tissue core did not contain tumor cells. Using Definiens Tissue Studio software, the staining intensity of brown chromogen of individual cells within the defined tumor ROI was quantified and categorized by visual analysis as negative, weak (AXL 1+), moderate (AXL 2+), or strong (AXL 3+). When more than 1 tissue core of a patient with NSCLC was included in the tumor TMA, the percentage of tumor cells in each staining intensity category (AXL negative, AXL 1+, AXL 2+, or AXL 3+) for that patient was calculated by adding up the number of tumor cells within that staining category in all tumor cores and dividing that number by the total number of tumor cells in all tumor cores. AXL H-score per NSCLC patient was calculated with the formula: (1 × % AXL^+ tumor cells 1+) + (2 × % AXL^+ tumor cells 2+) + (3 × % AXL^+ tumor cells 3+).

Kaplan-Meier plotter patient survival analysis. The publicly available KM plotter online tool contains data on 2437 lung cancer patients curated from Gene Expression Omnibus data sets, of which 1926 have OS data (21). AXL expression was evaluated using HGU133A or HGU133plus2 arrays (AXL: Affymetrix ID 202685a). The median AXL expression was used as the cutoff in the Cox regression analysis. The program generated survival plots with HRs, 95% CIs, and log-rank *P* value.

Western blot analysis. Cells were washed in ice-cold Tris-buffered saline and lysed in radioimmunoprecipitation assay buffer (10 nM Tris HCL at pH 8, 5 mM Na_2EDTA at pH 8, 1% NP-40, 0.5% sodium deoxycholate, 0.1% SDS), supplemented with phosphatase and protease inhibitors (Roche). Next, 5–40 μg protein was resolved on 4–12% RunBlue SDS-PAGE gels (Expedeon), transferred onto PVDF membranes (GE Healthcare Life Sciences), and blocked and incubated with AXL primary antibody (R&D Systems, AF154) at 4°C. Thereafter, the membranes were incubated with rabbit anti-goat (Merck) HRP-conjugated secondary antibodies at RT. The membranes were developed using Amersham ECL Prime Western Blotting Detecting Reagent (GE Healthcare Life Sciences) and CL-Xposure film (Thermo Fisher Scientific).

In vitro cytotoxicity assays. Cells were cultured to near confluence, after which cells were trypsinized and resuspended in culture medium. Cells were plated in a 96-well format at 2000 cells/well except for ER20, which were seeded at 5000 cells/well. Cells were allowed to adhere for 4 hours, and serial dilutions

of erlotinib, gefitinib, afatinib, osimertinib, enapotamab vedotin, or control-ADC were prepared in culture medium and added to the plates. Incubation of cells with 1 μM STAU (S6942-200, MilliporeSigma) was used as reference for 100% tumor cell kill, while untreated cells were used as reference for 100% cell growth. After 5 days of incubation at 37°C, 5% CO_2, CellTiter-Glo Reagent (Promega, G7571) was added to the wells up to a 10-fold dilution, and plates were incubated for 1.5 hours at 37°C, 5% CO_2. Subsequently, 180 μL/well was transferred to white 96-well Optiplate plates (PerkinElmer, 6005299), which were incubated for 30 minutes at RT. Finally, luminescence was measured on an EnVision multiplate reader (PerkinElmer). Viability was calculated as follows: % viability = (luminescence sample of interest – luminescence STAU) / (average luminescence of control vehicle treated – luminescence STAU), with STAU representing 1 μM STAU for 100% cell killing.

Mouse PDX clinical trial and in vivo studies. A mouse PDX clinical trial was performed by Crown Bioscience (Taicang, China; San Diego, California, USA). Female mice (4–8 weeks of age) were inoculated subcutaneously in the right flank with 1 tumor fragment (2–3 mm diameter), or 200 μL of cell suspension in ECM was subcutaneously injected in the right flank. Tumor volumes were measured at least twice per week using a digital caliper (Fowler). Tumor volumes (mm^3) were calculated as follows: tumor volume = 0.52 × length × $width^2$. Treatment was started when tumors reached 150–250 mm^3. For each of the 61 NSCLC PDX models evaluated, 1 xenografted mouse was used in the control (PBS) arm and 1 xenografted mouse in the treatment (enapotamab vedotin, 4 mg/kg) arm. Mice were injected intravenously with a 5 mL/kg test solution each, QWx2 on day 0 and 7 or day 1 and 8 after randomization. In most experiments, the body weight of the mice was monitored twice weekly, including on the day of treatment. Mice were observed at least 3 times weekly for clinical signs of illness. The experiment ended for individual mice when the tumor size exceeded 1.5 cm^3, the tumor showed severe ulceration, the mouse showed signs of serious clinical illness, tumor growth blocked the movement of the mouse, or tumor growth assessment had been completed. Evaluation of response to treatment with enapotamab vedotin was performed by comparing the ratio of the change in tumor volume of mice treated with enapotamab vedotin (ΔT) and the change in tumor volume of control mice (ΔC). Response was evaluated between day 7 and day 25, when exposure could reasonably be assumed. Models were excluded from the final analysis if the control tumor did not show at least doubling in tumor volume compared with day 0. Responding models (R) were defined as models showing ΔT/ΔC more than 10%, and NR models were defined as ΔT/ΔC more than 70%. The models that could not be classified as R or NR (10% < ΔT/ΔC < 70%) were classified as intermediate.

The expanded mouse experiments, performed in-house or by Crown Bioscience, Oncotest, or XenTech (see Table 1), involved *EGFR*–wild-type or -mutant NSCLC CDX or PDX models. All studies were performed using 7–10 female mice (aged 4–8 weeks) per group. Immunodeficient SCID or athymic nude mice were used in CDX studies, in which case tumors were induced by subcutaneous injection of 2 million to 5 million cells in 100–200 μL tumor cell suspension in the flank. For PDX models done by Charles River (Oncotest), animals under isoflurane anesthesia received unilateral tumor implants in the left flank. Models done at Crown Bioscience were implanted as stated above. Before treatment, mice were divided into groups of 7–10 mice each, with equal tumor size distribution (average and variance).

Treatments and measurements were performed as above, with the exception of CDX model LCLC-103H, in which mice were treated on the day of randomization only (day 0). Antitumor responses were classified into 4 categories (complete regression, regression, growth inhibition, no response) and determined at 2 weeks after the last treatment. An antitumor response was classified as complete regression when the tumor volume of a group reached 0 mm^3 within 2 weeks after the first treatment. An antitumor response was classified as regression when the average tumor volume of a group after 2 weeks was lower than the largest average tumor volume at the start of treatment. The growth inhibition classification was assigned to groups with an average tumor volume greater than at the start of treatment but still significantly lower than the average tumor volume in the control group (vehicle). The no response classification was assigned to groups with an average tumor volume that did not significantly differ from the control group (vehicle).

Analysis of mRNA expression by HTG EdgeSeq. FFPE tumors were analyzed for mRNA expression levels of AXL (as part of a panel of 2560 mRNAs) by targeted RNA sequencing using the HTG EdgeSeq Oncology Biomarker Panel. In brief, the tumor-containing area (delineated based on an H&E stain on an adjacent slide) was macrodissected from a single 5-μm FFPE slide and analyzed using the HTG EdgeSeq nuclease protection sequencing assay, as described elsewhere (55).

Flow cytometry analysis. For quantification of AXL expression on the cell surface, a Qifi quantification kit was used according to the manufacturer's instructions (DAKO). In brief, cells were stained with isotype control IgG1 (Pierce) or with the primary AXL antibody (ab89224, Abcam) for 30 minutes at 4°C, followed by a 30-minute incubation at 4°C with a secondary anti-mouse antibody (α-mouse FITC or APC from the Qifi kit was used). Next, cells were analyzed on a Fortessa flow cytometer (BD Biosciences). The number of AXL molecules on each cell was calculated using calibration beads from the Qifi kit according to according to the manufacturer's instructions.

Statistics. For analysis of clinical survival and AXL IHC, DFS and CSS were estimated by the Kaplan-Meier method, and the nonparametric log-rank test was applied to compare the different groups. Cox's multivariate regression model was applied with AXL H-score as covariate, obtaining HR and 95% CI. Significance levels of less than 0.10 in the univariate model were used to select variables for the Cox multivariate regression model. Correlations between IHC staining score and clinical and pathological characteristics were determined using Fisher's exact test. Each analysis was performed using a 2-sided 5% significance level and a 95% CI. Statistical analyses were performed using Stata version 15.

For in vivo PDX/CDX studies, differences in median tumor volumes were compared between treatment groups using nonparametric Mann-Whitney *U* tests with Bonferroni's post hoc tests to correct for multiple comparisons. Such analyses were performed on the last day that both groups were intact, but no later than day 25 after randomization, because PK studies indicated all administered drug was cleared by day 25 (data not shown). Mantel-Cox analysis of Kaplan-Meier curves was performed to analyze statistical differences in progression-free survival time with a general tumor size cutoff of 500 mm^3. Mice without detectable human IgG levels in the plasma were excluded from analysis.

Study approval. All animal procedures were approved and performed in accordance with guidelines provided by the Institutional Animal Care and Use Committee and US Department of Agriculture's Animal Welfare Act (9 CFR parts 1, 2, and 3) at Crown Bioscience Inc. (Beijing, China and San Diego, California, USA); The Direction Départementale de la Protection des Populations, Ministère de l'Agriculture et de l'Alimentation (Direction of the Veterinarian Services, Ministry of Agriculture and Food), France (XenTech, Evry, France); and the German Animal Welfare Act (Oncotest, Freiburg, Germany). For the IHC validation cohort of patients with NSCLC, approval from the Regional Committees on Health Research Ethics for Southern Denmark (Vejle, Denmark) and the Danish Data Protection Agency (Copenhagen, Denmark) was granted. All tissue samples were collected in compliance with informed consent policy.

Author contributions

LAK, MGT, KJ, AL, FDB, PWHIP, ECWB, and HJD designed research studies and interpreted data; MGT, KJ, EGVDH, and MB conducted experiments and acquired and analyzed data; LAK, MGT, GGZ and MLJ wrote the manuscript; UF and NP critically read the manuscript; MAZ coordinated the mouse clinical trial at Crown Bioscience; and ECWB and HJD supervised the research studies.

Acknowledgments

The authors would like to thank the patients who donated their tissues for this study, Laura Smits-De Vries for technical support at Genmab, Anette Rasmussen for technical support at University of Southern Denmark, Judith Klimovsky and Annette Ervin-Haynes for critical review of the manuscript, M. Kat Occhipinti for editorial assistance, and the technicians from the Division of Translational Oncology and Animal Center at Crown Bioscience, Oncotest, and XenTech for technical support of this work.

Address correspondence to: Henrik J. Ditzel, Institute of Molecular Medicine, University of Southern Denmark, J. B. Winsloewsvej 25, 5000 Odense, Denmark. Phone: 45-60113781; Email: hditzel@health.sdu.dk. Or to: Esther C.W. Breij, Genmab B.V., Uppsalalaan 15, 3584 CT Utrecht, the Netherlands; Phone: 31-302123123; Email: ebj@genmab.com.

PWHIP's present address is: Lava Therapeutics, Hertogenbosch, the Netherlands, and Department of Immunohematology and Blood Transfusion, Leiden University Medical Center, Leiden, the Netherlands.

1. Ferlay J, et al. Cancer incidence and mortality worldwide: sources, methods and major patterns in GLOBOCAN 2012. *Int J Cancer*. 2015;136(5):E359–E386.
2. Surveillance, Epidemiology, and End Results Program. Cancer Stat Facts: Lung and Bronchus Cancer. National Cancer Institute website. https://seer.cancer.gov/statfacts/html/lungb.html. Accessed October 1, 2019.
3. Gandhi L, et al. Pembrolizumab plus chemotherapy in metastatic non-small-cell lung cancer. *N Engl J Med*. 2018;378(22):2078–2092.
4. Rosell R, et al. Screening for epidermal growth factor receptor mutations in lung cancer. *N Engl J Med*. 2009;361(10):958–967.
5. Yang JCH, Janne PA, Ahn MJ, Horn L. EGFR gene mutations. In: Mok TS, Carbone DP, Hirsch FR, eds. *IASLC Atlas of EGFR Testing in Lung Cancer*. North Fort Myers, Florida, USA: Editorial Rx Press; 2012:25–44.
6. Mitsudomi T, et al. Gefitinib versus cisplatin plus docetaxel in patients with non-small-cell lung cancer harbouring mutations of the epidermal growth factor receptor (WJTOG3405): an open label, randomised phase 3 trial. *Lancet Oncol*. 2010;11(2):121–128.
7. Maemondo M, et al. Gefitinib or chemotherapy for non-small-cell lung cancer with mutated EGFR. *N Engl J Med*. 2010;362(25):2380–2388.
8. Byers LA, et al. An epithelial-mesenchymal transition gene signature predicts resistance to EGFR and PI3K inhibitors and identifies Axl as a therapeutic target for overcoming EGFR inhibitor resistance. *Clin Cancer Res*. 2013;19(1):279–290.
9. Zhang Z, et al. Activation of the AXL kinase causes resistance to EGFR-targeted therapy in lung cancer. *Nat Genet*. 2012;44(8):852–860.
10. Aguilera TA, et al. Reprogramming the immunological microenvironment through radiation and targeting Axl. *Nat Commun*. 2016;7:13898.
11. Hugo W, et al. Genomic and transcriptomic features of response to anti-PD-1 therapy in metastatic melanoma. *Cell*. 2016;165(1):35–44.
12. Wang C, et al. Gas6/Axl axis contributes to chemoresistance and metastasis in breast cancer through Akt/GSK-3β/β-catenin signaling. *Theranostics*. 2016;6(8):1205–1219.
13. Gay CM, Balaji K, Byers LA. Giving AXL the axe: targeting AXL in human malignancy. *Br J Cancer*. 2017;116(4):415–423.
14. Rosell R, et al. Erlotinib versus standard chemotherapy as first-line treatment for European patients with advanced EGFR mutation-positive non-small-cell lung cancer (EURTAC): a multicentre, open-label, randomised phase 3 trial. *Lancet Oncol*. 2012;13(3):239–246.
15. Jacobsen K, et al. Convergent Akt activation drives acquired EGFR inhibitor resistance in lung cancer. *Nat Commun*. 2017;8(1):410.
16. Kobayashi S, et al. EGFR mutation and resistance of non-small-cell lung cancer to gefitinib. *N Engl J Med*. 2005;352(8):786–792.
17. Pao W, et al. Acquired resistance of lung adenocarcinomas to gefitinib or erlotinib is associated with a second mutation in the EGFR kinase domain. *PLoS Med*. 2005;2(3):e73.
18. Turke AB, et al. Preexistence and clonal selection of MET amplification in EGFR mutant NSCLC. *Cancer Cell*. 2010;17(1):77–88.
19. Xie S, et al. Mer receptor tyrosine kinase is frequently overexpressed in human non-small cell lung cancer, confirming resistance to erlotinib. *Oncotarget*. 2015;6(11):9206–9219.
20. Boshuizen J, et al. Cooperative targeting of melanoma heterogeneity with an AXL antibody-drug conjugate and BRAF/MEK inhibitors. *Nat Med*. 2018;24(2):203–212.
21. Győrffy B, Surowiak P, Budczies J, Lánczky A. Online survival analysis software to assess the prognostic value of biomarkers using transcriptomic data in non-small-cell lung cancer. *PLoS ONE*. 2013;8(12):e82241.
22. Namba K, et al. Activation of AXL as a preclinical acquired resistance mechanism against osimertinib treatment in *EGFR*-mutant non-small cell lung cancer cells. *Mol Cancer Res*. 2019;17(2):499–507.
23. Tian Y, et al. Anexelekto (AXL) increases resistance to EGFR-TKI and activation of AKT and ERK1/2 in non-small cell lung cancer cells. *Oncol Res*. 2016;24(5):295–303.
24. Tschuch C, et al. Abstract A10: establishment and characterization of a patient-derived non-small cell lung cancer mouse model of acquired resistance towards anti-EGFR treatment. *Mol Cancer Ther*. 2015;14(12):Supplment 2.
25. Soria JC, et al. Osimertinib in untreated EGFR-mutated advanced non-small-cell lung cancer. *N Engl J Med*. 2018;378(2):113–125.
26. Oxnard GR, et al. Assessment of resistance mechanisms and clinical implications in patients with EGFR T790M-positive lung cancer and acquired resistance to osimertinib. *JAMA Oncol*. 2018;4(11):1527–1534.
27. Déas O. BL, et al. Development of preclinical models to accelerate the identification of next generation treatments for patients with acquired resistance to targeted therapies. Paper presented at AACR Annual Meeting 2018; April 14–18, 2018; Chicago, Illinois, USA. https://cancerres.aacrjournals.org/content/78/13_Supplement/2147.
28. Planchard D, et al. EGFR-independent mechanisms of acquired resistance to AZD9291 in EGFR T790M-positive NSCLC patients. *Ann Oncol*. 2015;26(10):2073–2078.
29. Socinski MA, et al. Atezolizumab for first-line treatment of metastatic nonsquamous NSCLC. *N Engl J Med*. 2018;378(24):2288–2301.
30. Yu S, et al. HOXA4-dependent transcriptional activation of AXL promotes cisplatin- resistance in lung adenocarcinoma cells. *Anticancer Agents Med Chem*. 2018;18(14):2062–2067.
31. Scaltriti M, Elkabets M, Baselga J. Molecular pathways: AXL, a membrane receptor mediator of resistance to therapy. *Clin Cancer Res*. 2016;22(6):1313–1317.
32. Debruyne DN, et al. ALK inhibitor resistance in ALK(F1174L)-driven neuroblastoma is associated with AXL activation and induction of EMT. *Oncogene*. 2016;35(28):3681–3691.
33. Karachaliou N, et al. Common co-activation of AXL and CDCP1 in EGFR-mutation-positive non-smallcell lung cancer associated with poor prognosis. *EBioMedicine*. 2018;29:112–127.
34. Ishikawa M, et al. Higher expression of receptor tyrosine kinase Axl, and differential expression of its ligand, Gas6, predict poor survival in lung adenocarcinoma patients. *Ann Surg Oncol*. 2013;20 Suppl 3:S467–S476.
35. Seike M, et al. AXL and GAS6 co-expression in lung adenocarcinoma as a prognostic classifier. *Oncol Rep*. 2017;37(6):3261–3269.
36. Liu YN, et al. Acquired resistance to EGFR tyrosine kinase inhibitors is mediated by the reactivation of STC2/JUN/AXL signaling in lung cancer. *Int J Cancer*. 2019;145(6):1609–1624.
37. Zhang G, Wang M, Zhao H, Cui W. Function of Axl receptor tyrosine kinase in non-small cell lung cancer. *Oncol Lett*. 2018;15(3):2726–2734.

38. Wu F, Li J, Jang C, Wang J, Xiong J. The role of Axl in drug resistance and epithelial-to-mesenchymal transition of non-small cell lung carcinoma. *Int J Clin Exp Pathol*. 2014;7(10):6653–6661.
39. Linger RM, et al. Mer or Axl receptor tyrosine kinase inhibition promotes apoptosis, blocks growth and enhances chemosensitivity of human non-small cell lung cancer. *Oncogene*. 2013;32(29):3420–3431.
40. Lay JD, et al. Sulfasalazine suppresses drug resistance and invasiveness of lung adenocarcinoma cells expressing AXL. *Cancer Res*. 2007;67(8):3878–3887.
41. Jenkins RW, Barbie DA, Flaherty KT. Mechanisms of resistance to immune checkpoint inhibitors. *Br J Cancer*. 2018;118(1):9–16.
42. Graham DK, DeRyckere D, Davies KD, Earp HS. The TAM family: phosphatidylserine sensing receptor tyrosine kinases gone awry in cancer. *Nat Rev Cancer*. 2014;14(12):769–785.
43. Rothlin CV, Ghosh S, Zuniga EI, Oldstone MB, Lemke G. TAM receptors are pleiotropic inhibitors of the innate immune response. *Cell*. 2007;131(6):1124–1136.
44. Taniguchi H, et al. AXL confers intrinsic resistance to osimertinib and advances the emergence of tolerant cells. *Nat Commun*. 2019;10(1):259.
45. Le X, et al. Landscape of EGFR-dependent and -independent resistance mechanisms to osimertinib and continuation therapy beyond progression in *EGFR*-mutant NSCLC. *Clin Cancer Res*. 2018;24(24):6195–6203.
46. Piotrowska Z, et al. Landscape of acquired resistance to osimertinib in *EGFR*-mutant NSCLC and clinical validation of combined EGFR and RET inhibition with osimertinib and BLU-667 for acquired *RET* fusion. *Cancer Discov*. 2018;8(12):1529–1539.
47. Schmid S, et al. Patterns of progression on osimertinib in EGFR T790M positive NSCLC: a Swiss cohort study. *Lung Cancer*. 2019;130:149–155.
48. Zhang YC, et al. Analysis of resistance mechanisms to abivertinib, a third-generation EGFR tyrosine kinase inhibitor, in patients with EGFR T790M-positive non-small cell lung cancer from a phase I trial. *EBioMedicine*. 2019;43:180–187.
49. Amann J, et al. Aberrant epidermal growth factor receptor signaling and enhanced sensitivity to EGFR inhibitors in lung cancer. *Cancer Res*. 2005;65(1):226–235.
50. Cross DA, et al. AZD9291, an irreversible EGFR TKI, overcomes T790M-mediated resistance to EGFR inhibitors in lung cancer. *Cancer Discov*. 2014;4(9):1046–1061.
51. Koizumi F, Shimoyama T, Taguchi F, Saijo N, Nishio K. Establishment of a human non-small cell lung cancer cell line resistant to gefitinib. *Int J Cancer*. 2005;116(1):36–44.
52. Kurokawa M, Ise N, Omi K, Goishi K, Higashiyama S. Cisplatin influences acquisition of resistance to molecular-targeted agents through epithelial-mesenchymal transition-like changes. *Cancer Sci*. 2013;104(7):904–911.
53. Sos ML, et al. PTEN loss contributes to erlotinib resistance in EGFR-mutant lung cancer by activation of Akt and EGFR. *Cancer Res*. 2009;69(8):3256–3261.
54. Pøhl M, Olsen KE, Holst R, Ditzel HJ, Hansen O. Tissue microarrays in non-small-cell lung cancer: reliability of immunohistochemically-determined biomarkers. *Clin Lung Cancer*. 2014;15(3):222–230.e3.
55. Girard L, et al. An expression signature as an aid to the histologic classification of non-small cell lung cancer. *Clin Cancer Res*. 2016;22(19):4880–4889.